Simulations of momentum correlation functions of light (anti)nuclei in relativistic heavy-ion collisions at $\sqrt{s_{NN}} = 39$ GeV

Ting-Ting Wang(王婷婷),[1] Yu-Gang Ma(马余刚) [iD] ,[1, 2, *] and Song Zhang(张松) [iD] [1, 2]

[1]*Key Laboratory of Nuclear Physics and Ion-Beam Application (MOE),*
Institute of Modern Physics, Fudan University, Shanghai 200433, China
[2]*Shanghai Research Center for Theoretical Nuclear Physics, NSFC and Fudan University, Shanghai 200438, China*
(Dated: September 18, 2022)

Momentum correlation functions of light (anti)nuclei formed by the coalescence mechanism of (anti)nucleons are calculated in several relativistic heavy-ion collision systems, namely $^{10}_{5}$B $+^{10}_{5}$ B, $^{16}_{8}$O $+^{16}_{8}$ O, $^{40}_{20}$Ca $+^{40}_{20}$ Ca as well as $^{197}_{79}$Au $+^{197}_{79}$ Au, at different centralities at center of mass energy $\sqrt{s_{NN}} = 39$ GeV within the framework of A Multi-Phase Transport (AMPT) model complemented by the Lednický and Lyuboshitz analytical method. Momentum correlation functions for identical or nonidentical light (anti)nuclei are constructed in the above collision systems at so high collision energy. The results suggest that emission of light (anti)nuclei occurs from a source of smaller space-time extent in more peripheral collisions. The effect of system-size on the momentum correlation functions of identical or nonidentical light (anti)nuclei is also explored in several central collisions. The results indicate that the emission source-size of light (anti)nuclei pairs deduced from their momentum correlation functions and system-size is self-consistent. Momentum correlation functions of nonidentical light nuclei pairs gated on velocity are applied to infer the average emission sequence of them. The results indicate that protons are emitted in average on a similar time scale with neutrons but earlier than deuterons or tritons in the small relative momentum region. In addition, larger interval of the average emission order among them is observed by large centrality and smaller system collisions.

I. INTRODUCTION

In heavy-ion collisions (HICs), two-particle correlation function is different from the original application in astronomy [1, 2], and has been normally utilized to extract space-time information of the emission source and probe the dynamical evolution of nuclear collisions in an extensive energy range [3–12]. Many different studies on the two-particle momentum correlation functions in intermediate energy HICs can be also found in literature, eg. Refs. [11, 13–25], which include the momentum correlation functions of neutron, proton as well as light charged particle (LCP) pairs. Multi-variable dependences of the momentum correlation functions, such as impact parameters, total momentum of particle pairs, isospin of the emission source, nuclear symmetry energy, nuclear equation of state (EOS) as well as in-medium nucleon-nucleon cross section (NNCS) etc., contain a wealth of information about the space-time characteristics of intermediate energy HICs. In high energy HICs, two-hadron momentum correlation functions, also called as Hanbury Brown-Twiss (HBT) interferometry, were also well measured and some interesting properties on emission source were extracted [26, 27]. Oscillations of the extracted HBT radii versus emission angle indicate sources elongated perpendicular to the reaction plane. The results indicate that initial shape could be remained to be identified even though the pressure and expansion the collision system. Furthermore, interaction between

antiprotons has been also measured with the momentum correlation functions and the equality of interactions between p-p and $\bar{p}$-$\bar{p}$ was approved by the STAR Collaboration [28]. The interaction property of the particle pairs has been discussed for other particles, for instance Λ pairs [29], proton-Ω and proton-Ξ etc [30, 31], with the same momentum correlation technique. Furthermore, the measurements of momentum correlation functions for nonidentical nucleons and light clusters can be used to characterize the mean emission sequence of them, which was firstly proposed in Ref. [32]. Theoretical study has been extended to different kinds of nonidentical particle pairs, for instance p-d, n-p [33–36], π-p [37], K^{+}-K^{-} [38], d-t [11, 22] as well as ^{3}He-α particles [39] in intermediate energy HICs.

In this work we extend, for the first time, the momentum correlation functions of light (anti)nuclei to ultra-relativistic heavy-ion collisions simulated by A Multi-Phase Transport (AMPT) model [40, 41] coupled with a dynamical coalescence model [42–44], specifically at $\sqrt{s_{NN}} = 39$ GeV. Different gating conditions such as centrality gates, system-size gates as well as velocity gates are applied to the momentum correlation functions of light (anti)nuclei pairs. In particular, we report on the indication of the emission chronology of protons, deuterons and tritons which can be deduced from their corresponding momentum correlation functions in ultra-relativistic HICs at $\sqrt{s_{NN}} = 39$ GeV. The emission sequence inferred from the correlation functions is expected measurable in future experiments to verify our deduction from the coalescence picture.

The rest of this article is organized as follows. In Section II A and II B, we briefly describe A Multi-Phase

Transport model [40, 41] and the coalescence model [42–44], then introduce how to calculate the momentum correlation functions of particle pairs by using the Lednický and Lyuboshitz analytical formalism [3, 45–48] in Section II C. In Section III, we summarize the simulated results of the light (anti)nuclei momentum correlation functions gated on various parameters in relativistic heavy-ion collisions. Section III A compares the results of proton-proton and proton-antiproton momentum correlation functions with experimental data from the RHIC-STAR collaboration. From Section III B to III D, identical and nonidentical light (anti)nuclei momentum correlation functions gated on different conditions are systematically discussed, respectively. Finally, a summary and outlook are given in Section IV.

II. MODELS AND FORMALISM

A. AMPT model

To obtain phase-space distributions of (anti)particles, A Multi-Phase Transport model [40, 41] is used as the event generator, which has been applied successfully for studying heavy-ion collisions at relativistic energies, eg. [43, 44, 49–57]. We briefly review the main components of the AMPT model used in the present work. In the version of AMPT, the initial phase-space information of partons is generated by the heavy-ion jet interaction generator (HIJING) model [58, 59]. The interaction between partons is then simulated by Zhang's parton cascade (ZPC) model [60]. During the hadronization process, a quark coalescence model is used to combine partons into hadrons [61–63]. Then, the hadronic rescattering evolution is described by a relativistic transport (ART) model [64].

In this paper, the collisions of $_{5}^{10}$B $+_{5}^{10}$ B, $_{8}^{16}$O $+_{8}^{16}$ O, $_{20}^{40}$Ca $+_{20}^{40}$ Ca for the $0-10$ % central collisions at mid-rapidity ($|y| < 0.5$) as well as $_{79}^{197}$Au $+_{79}^{197}$ Au at same mid-rapidity for five centralities of $0-10$ %, $10-20$ %, $20-40$ %, $40-60$ %, and $60-80$ % at $\sqrt{s_{NN}}$ = 39 GeV are simulated. The phase-space distributions of (anti)particles are selected at the final stage in the hadronic rescattering process (ART model [64]) with considering baryon-baryon, baryon-meson, and meson-meson elastic and inelastic scatterings, as well as resonance decay or week decay. The transverse momentum spectra of light (anti)nuclei have been successfully reproduced by the AMPT model with the maximum hadronic rescattering time of 100 fm/c [44]. Therefore, the same maximum hadronic rescattering time is used for the most calculations in this work except for a quantitative comparison with a preliminary p-p and p-$\bar{p}$ data from the STAR collaboration in Sec. III A.

B. Coalescence model

In our model calculations, light (anti)clusters such as (anti)deuterons and tritons are constructed by using the coalescence model as follows [65, 66]. The coalescence model has been used widely in describing the production of light clusters in the intermediate [67–71] and high energies [72, 73] heavy-ion collisions. In the model, the probability for producing M-nucleon cluster is determined by its Wigner phase-space density and the nucleon phase-space distribution at the freeze-out stage [42]. The multiplicity of an M-nucleon cluster in transport model simulations for heavy-ion collisions is given by,

$$N_M = G \int \sum_{i_1 > i_2 > \cdots > i_M} d\vec{r}_{i_1} d\vec{k}_{i_1} \cdots d\vec{r}_{i_{M-1}} d\vec{k}_{i_{M-1}}$$
$$\left\langle \rho_i^W \left(\vec{r}_{i_1}, \vec{k}_{i_1}, \cdots, \vec{r}_{i_{M-1}}, \vec{k}_{i_{M-1}} \right) \right\rangle \quad (1)$$

where $\vec{r}_{i_1}, \vec{r}_{i_{M-1}}$ and $\vec{k}_{i_1}, \vec{k}_{i_{M-1}}$ are the relative coordinates and momentum in the M-nucleon rest frame, and spin-isospin statistical factor G is 3/8 for (anti)deuteron and 1/3 for triton [42]. In addition, ρ^W is the Wigner density function, which is different for all kinds of particles. Therefore, we will calculate separately the Wigner phase-space density of (anti)deuteron and triton in detail. The Wigner phase-space density of (anti)deuteron is constructed by,

$$\rho_d^W(\vec{r}, \vec{k}) = 8 \sum_{i=1}^{15} c_i^2 \exp\left(-2\omega_i r^2 - \frac{k^2}{2\omega_i}\right)$$
$$+ 16 \sum_{i>j}^{15} c_i c_j \left(\frac{4\omega_i \omega_j}{(\omega_i + \omega_j)^2}\right)^{\frac{3}{4}} \exp\left(-\frac{4\omega_i \omega_j}{\omega_i + \omega_j} r^2\right)$$
$$\times \exp\left(-\frac{k^2}{\omega_i + \omega_j}\right) \cos\left(2\frac{\omega_i - \omega_j}{\omega_i + \omega_j} \vec{r} \cdot \vec{k}\right) \quad (2)$$

where $\vec{k} = \left(\vec{k}_1 - \vec{k}_2\right)/2$ is the relative momentum and $\vec{r} = (\vec{r}_1 - \vec{r}_2)$ is the relative coordinate of (anti)proton and (anti)neutron. The Wigner phase-space density of triton is constructed by a spherical harmonic oscillator [42, 43, 74],

$$\rho_t^W\left(\rho, \lambda, \vec{k}_\rho, \vec{k}_\lambda\right)$$
$$= \int \psi\left(\rho + \frac{\vec{R}_1}{2}, \lambda + \frac{\vec{R}_2}{2}\right) \psi^*\left(\rho - \frac{\vec{R}_1}{2}, \lambda - \frac{\vec{R}_2}{2}\right)$$
$$\times \exp\left(-i\vec{k}_\rho \cdot \vec{R}_1\right) \exp\left(-i\vec{k}_\lambda \cdot \vec{R}_2\right) 3^{\frac{3}{2}} d\vec{R}_1 d\vec{R}_2$$
$$= 8^2 \exp\left(-\frac{\rho^2 + \lambda^2}{b^2}\right) \exp\left(-\left(\vec{k}_\rho^2 + \vec{k}_\lambda^2\right) b^2\right) \quad (3)$$

where ρ and λ are relative coordinates, $\vec{k}_\rho$ and $\vec{k}_\lambda$ are the relative momenta in the Jacobi coordinate.

The above parameters of the Gaussian fit coefficient c_i and w_i for (anti)deuteron as well as b for triton are given in Ref. [42]. Based on the phase-space information of light (anti)cluster obtained by the above coalescence model, the momentum correlation functions of (non)identical light (anti)cluster pairs can be discussed in the following of this paper.

C. Lednický́nd Lyuboshitz technique

Finally, we briefly review the technique of the two-particle momentum correlation function proposed by Lednický and Lyuboshitz [45–47]. The method calculating the two-particle momentum correlation function in heavy-ion collisions is based on the principle as follows: when two particles are emitted at small relative momentum, their momentum correlation function is determined by the space-time characteristics of the production processes owing to the effects of quantum statistics and final-state interactions [3, 48]. Therefore, the two-particle momentum correlation function can be expressed through a square of the symmetrizied Bethe-Salpeter amplitude averaging over the four coordinates of the emitted particles and the total spin of the two-particle system, which represents the continuous spectrum of the two-particle state. In the method, the final-state interaction of the particle pairs is assumed independent in the production process. According to the conditions in Ref. [33], the momentum correlation function of two particles can be written as the expression:

$$\mathbf{C}(k^*) = \frac{\int \mathbf{S}(\mathbf{r}^*, \mathbf{k}^*)\, |\Psi_{\mathbf{k}^*}(\mathbf{r}^*)|^2 \, d^4\mathbf{r}^*}{\int \mathbf{S}(\mathbf{r}^*, \mathbf{k}^*)\, d^4\mathbf{r}^*}, \quad (4)$$

where $\mathbf{r}^* = \mathbf{x}_1 - \mathbf{x}_2$ is the relative distance of the two particles in the pair rest frame at their kinetic freeze-out, $\mathbf{k}^*$ is half of the relative momentum between two particles in the pair rest frame, $\mathbf{S}(\mathbf{r}^*, \mathbf{k}^*)$ is the probability to emit a particle pair with given $\mathbf{r}^*$ and $\mathbf{k}^*$, i.e., the source emission function, and $\Psi_{\mathbf{k}^*}(\mathbf{r}^*)$ is the reduced Bethe-Salpeter amplitude which can be approximated by the outer solution of the scattering problem [28, 75]. This approximation is valid on condition $|t^*| \ll m(r^*)^2$, which is well fulfilled for sufficiently heavy particles like protons or kaons and reasonably fulfilled even for pions [46]. In the above limit, the asymptotic solution of the wave function of the two charged particles approximately takes the expression:

$$\Psi_{\mathbf{k}^*}(\mathbf{r}^*) = e^{i\delta_c}\sqrt{A_c(\lambda)} \times$$
$$\left[e^{-i\mathbf{k}^*\mathbf{r}^*} F(-i\lambda, 1, i\xi) + f_c(k^*)\frac{\tilde{G}(\rho,\lambda)}{r^*} \right]. \quad (5)$$

In the above equation, $\delta_c = arg\,\Gamma(1 + i\lambda)$ is the Coulomb s-wave phase shift with $\lambda = (k^* a_c)^{-1}$ where a_c is the two-particle Bohr radius, $A_c(\lambda) = 2\pi\lambda\left[\exp(2\pi\lambda) - 1\right]^{-1}$ is the Coulomb penetration factor, and its positive (negative) value corresponds to the repulsion (attraction). $\tilde{G}(\rho,\lambda) = \sqrt{A_c(\lambda)}\left[G_0(\rho,\lambda) + iF_0(\rho,\lambda)\right]$ is a combination of regular (F_0) and singular (G_0) s-wave Coulomb functions [46, 47]. $F(-i\lambda, 1, i\xi) = 1 + (-i\lambda)(i\xi)/1!^2 + (-i\lambda)(-i\lambda + 1)(i\xi)^2/2!^2 + \cdots$ is the confluent hypergeometric function with $\xi = \mathbf{k}^*\mathbf{r}^* + \rho$, $\rho = k^* r^*$.

$$f_c(k^*) = \left[K_c(k^*) - \frac{2}{a_c}h(\lambda) - ik^* A_c(\lambda) \right]^{-1} \quad (6)$$

$f_c(k^*)$ is the s-wave scattering amplitude renormalizied by the long-range Coulomb interaction, with $h(\lambda) = \lambda^2 \sum_{n=1}^{\infty}\left[n(n^2 + \lambda^2)\right]^{-1} - C - \ln[\lambda]$ where $C = 0.5772$ is the Euler constant. $K_c(k^*) = \frac{1}{f_0} + \frac{1}{2}d_0 k^{*2} + Pk^{*4} + \cdots$ is the effective range function, where d_0 is the effective radius of the strong interaction, f_0 is the scattering length and P is the shape parameter. The parameters of the effective range function are important parameters characterizing the essential properties of the final-state interactions, and can be extracted from the correlation function measured experimentally [28, 34, 76, 77]. Table I shows the parameters of the effective range function for different particle pairs in the present work.

TABLE I. Experimental determination of the effective range function parameters for n-n ($\bar{n}$-$\bar{n}$), p-p ($\bar{p}$-$\bar{p}$), t-t, n-p ($\bar{n}$-$\bar{p}$), p-d ($\bar{p}$-$\bar{d}$), p-t and d-t systems [28, 76, 77].

System	Spin	$f_0\ (fm)$	$d_0\ (fm)$	$P\ (fm^3)$
n-n ($\bar{n}$-$\bar{n}$)	0	17	2.7	0.0
p-p ($\bar{p}$-$\bar{p}$)	0	7.8	2.77	0.0
t-t	0	1×10^{-6}	0.0	0.0
n-p ($\bar{n}$-$\bar{p}$)	0	23.7	2.7	0.0
p-d ($\bar{p}$-$\bar{d}$)	1/2	-2.73	2.27	0.08
	3/2	-11.88	2.63	-0.54
p-t	0	1×10^{-6}	0.0	0.0
d-t	0	1×10^{-6}	0.0	0.0

In the above table, for n-n ($\bar{n}$-$\bar{n}$) and n-p ($\bar{n}$-$\bar{p}$) momentum correlation functions which include uncharged particle, the Coulomb penetration factor ($A_c(\lambda)$) is not considered and only the short-range particle interaction works. For the momentum correlation functions of charged particles such as p-$\bar{p}$, p-p ($\bar{p}$-$\bar{p}$), d-d ($\bar{d}$-$\bar{d}$), t-t, p-d ($\bar{p}$-$\bar{d}$), p-t and d-t, both the Coulomb interaction and the short-range interaction dominated by the s-wave interaction are taken into account. The momentum correlation function of p-p ($\bar{p}$-$\bar{p}$) particle pairs is

dominately contributed by only the singlet ($S = 0$) s-wave final-state interactions while both spins $1/2$ and $3/2$ contribute in the case of p-d ($\bar{p}$-$\bar{d}$) system. Moreover, for (anti)deuteron-(anti)deuteron momentum correlation function, a parametrization of the s-wave phase shifts δ has been used from the solution of $K_c(k^*) = \cot\delta$ for each total pair spin $S = 0, 1, 2$. Note that the effective range function for the total spin $S = 1$ is irrelevant, since it does not contribute due to the quantum statistics symmetrization.

III.   ANALYSIS AND DISCUSSION

A.   Comparison between our simulations and preliminary data

Fig. 1 presents results of p-p and p-$\bar{p}$ correlation functions for three different centrality classes of $0 - 10$ %, $10 - 30$ %, and $30 - 70$ % calculated by the AMPT model in Au + Au collisions at $\sqrt{s_{NN}} = 39$ GeV. Within the cut of transverse momentum p_t and rapidity y, we confront the experimental data with the predictions of the AMPT model combined with Lednický and Lyuboshitz code. When the phase-space information of nucleons at the maximum hadronic rescattering time of 700 fm/c is selected from the AMPT model, it is found that the results can well describe the experimental data for the momentum correlation functions of p-p and p-$\bar{p}$ from the RHIC-STAR collaboration [78, 79], especially in more central collisions. Considering that the preliminary experimental results were not corrected by feed-down effect corrections [78, 79], the real correlation functions for primary p-p and p-$\bar{p}$ could be much more stronger. In this case, using much longer hadronic rescattering time of 700 fm/c in the AMPT model might be a reasonable choice for making quantitative comparison with feed-down uncorrected data since the system will become more expanded and weakly correlated among particles after longer hadronic rescattering time in AMPT. However, the quantitative reproduction is not our main concern in the present work. In the following calculations, we fixed the maximum hadronic rescattering time at 100 fm/c and presented systematic results among different light (anti)nuclei.

B.   Centrality and system-size dependence of identical light (anti)nuclei momentum correlation functions

The centrality dependence of the two-particle momentum correlation function can systematically investigate the contributions from the system-size and particle interactions on the correlations. Fig. 2 (a) and (c) presents the momentum correlation functions of identical (anti)particle pairs (n-n ($\bar{n}$-$\bar{n}$) and p-p ($\bar{p}$-$\bar{p}$)) for $^{197}_{79}$Au $+^{197}_{79}$Au collisions at different centralities of $0 - 10$
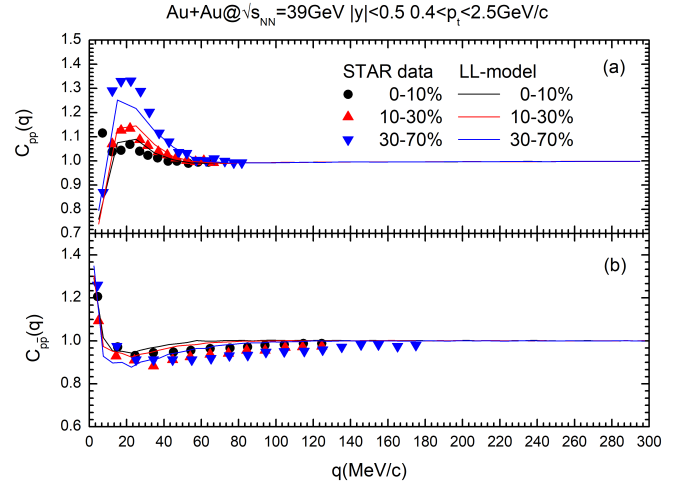

FIG. 1.   Proton-proton (a) and proton-antiproton (b) momentum correlation functions for different centrality classes in $\sqrt{s_{NN}} = 39$ GeV Au + Au collisions. Solid markers represent the preliminary experimental data from the RHIC-STAR collaboration [78, 79], and lines represent our model calculation results from the AMPT model plus the Lednický and Lyuboshitz code. Note that the longer hadronic rescattering time of 700 fm/c is used in this specific calculation in comparison with the data.

%, $10 - 20$ %, $20 - 40$ %, $40 - 60$ %, and $60 - 80$ % at $\sqrt{s_{NN}} = 39$ GeV. The momentum correlation functions of (anti)neutron pairs exhibit more than unity in Fig. 2 (a), which is caused by the attractive s-wave interaction between the two (anti)neutrons. In Fig. 2 (c), the shape of the (anti)proton$-$(anti)proton momentum correlation functions looks as expected from the interplay between the quantum statistical (QS) and final state interactions (FSI) and is consistent with previous results [13, 28, 34]. The (anti)proton$-$(anti)proton momentum correlation functions exhibit less than unity at low relative momentum q in Fig. 2 (c), which is mainly caused by the Coulomb repulsion between the (anti)proton pairs. With increasing relative momentum, the attractive s-wave interaction between the two (anti)protons gives rise to a maximum of the (anti)proton$-$(anti)proton momentum correlation functions at q around 0.020 GeV in Fig. 2 (c). The antiproton$-$antiproton momentum correlation functions show a similar structure with proton pairs, resulting from the same attractive interaction between two antiprotons [28]. Fig. 2 (a) and (c) compare five centralities of $0 - 10$ %, $10 - 20$ %, $20 - 40$ %, $40 - 60$ %, and $60 - 80$ % of the two-(anti)particle momentum correlation functions. The enhancement strength of the n-n ($\bar{n}$-$\bar{n}$) and p-p ($\bar{p}$-$\bar{p}$) momentum correlation functions is observed in peripheral selection. These results indicate that (anti)particle emission occurs from a source of smaller space$-$time extent in peripheral collision. In addition, the effect of system$-$size on the momentum correlation functions of (anti)particles is also investigated by four different systems, namely $^{10}_5$B $+^{10}_5$B, $^{16}_8$O $+^{16}_8$O, $^{40}_{20}$Ca $+^{40}_{20}$Ca

and $^{197}_{79}\mathrm{Au}+^{197}_{79}\mathrm{Au}$, in central collisions. In Fig. 2 (b) and (d), the n-n ($\bar{n}$-$\bar{n}$) and p-p ($\bar{p}$-$\bar{p}$) momentum correlation functions appear very sensitive to system-size and an enhancement strength is observed when particle pairs emitted from smaller system collisions. This enhancement strength of the momentum correlation functions for particle pairs is a physical effect stemming from the smaller space−time extent of the emission source [8]. Therefore, the emission source-size of particle pairs obtained by their momentum correlation functions and system-size is self-consistent.
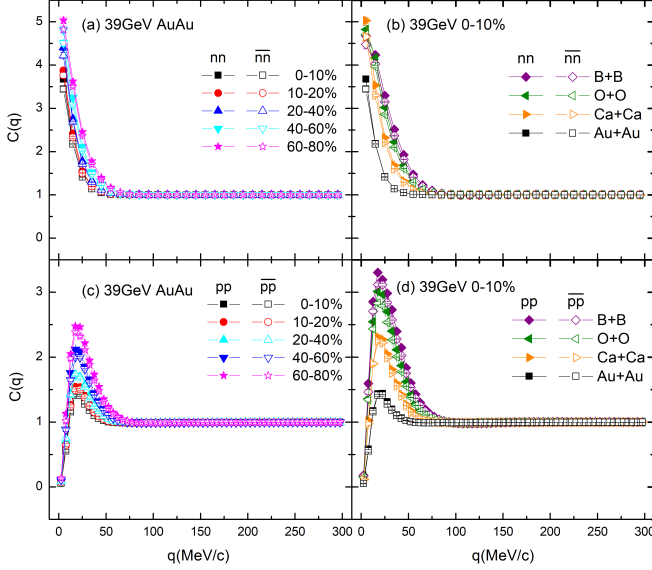
FIG. 2. The momentum correlation functions at mid-rapidity ($|y| < 0.5$) of (anti)neutron-pairs and (anti)proton-pairs as a function of five different centralities for $^{197}_{79}\mathrm{Au}+^{197}_{79}\mathrm{Au}$ reaction at $\sqrt{s_{NN}} = 39$ GeV are presented in (a) and (c), respectively. The momentum correlation functions of (anti)neutron-pairs and (anti)proton-pairs at mid-rapidity ($|y| < 0.5$) for 0-10% central collisions of $^{10}_{5}\mathrm{B}+^{10}_{5}\mathrm{B}$, $^{16}_{8}\mathrm{O}+^{16}_{8}\mathrm{O}$, $^{40}_{20}\mathrm{Ca}+^{40}_{20}\mathrm{Ca}$ as well as $^{197}_{79}\mathrm{Au}+^{197}_{79}\mathrm{Au}$ systems at $\sqrt{s_{NN}} = 39$ GeV are presented in (b) and (d), respectively. The p-p and n-n momentum correlation functions (solid symbols) and the anti-one (open symbols) are shown in each panel.

Figure 3 shows the centrality and system-size dependences of the momentum correlation functions for light (anti)cluster in similar condition as in Fig. 2. Figure 3 (a) and (c) present the momentum correlation functions of d-d ($\bar{d}$-$\bar{d}$) and t-t for $^{197}_{79}\mathrm{Au}+^{197}_{79}\mathrm{Au}$ collisions at different centralities of $0 - 10$ %, $10 - 20$ %, $20 - 40$ %, $40 - 60$ %, and $60 - 80$ % at $\sqrt{s_{NN}} = 39$ GeV. The d-d ($\bar{d}$-$\bar{d}$) momentum correlation functions exhibit less than unity at lower relative momentum q in Fig. 3 (a) and (b), which is caused by the Coulomb repulsion. Then, with increasing relative momentum q, the anti-correlation between two-(anti)deuteron pairs is more complex. The two-triton momentum correlation functions are less than unity with increasing relative momentum q as shown in Fig. 2 (c) and (d), which is caused by only the Coulomb potential in the Lednický and Lyuboshitz code [45–47].
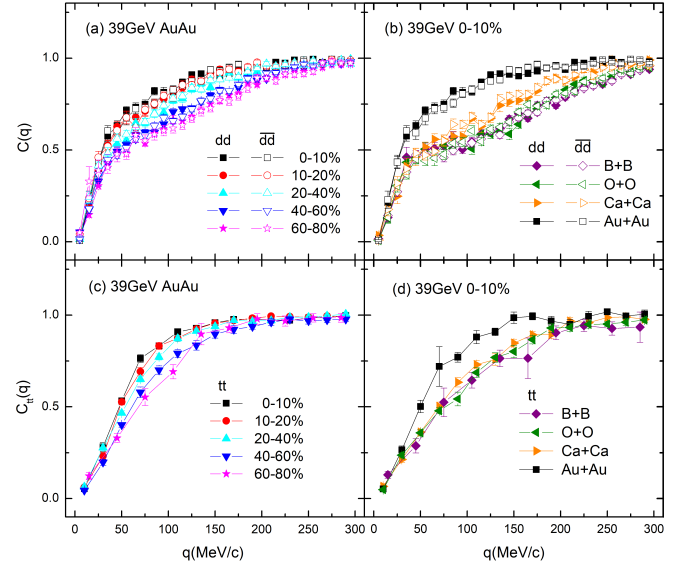

FIG. 3. Similar to Fig. 2 but for the light (anti)cluster pairs. (a) (b) $d - d$ momentum correlation functions (solid symbols) and the anti-one (open symbols), (c) (d) $t - t$ momentum correlation functions (solid symbols).
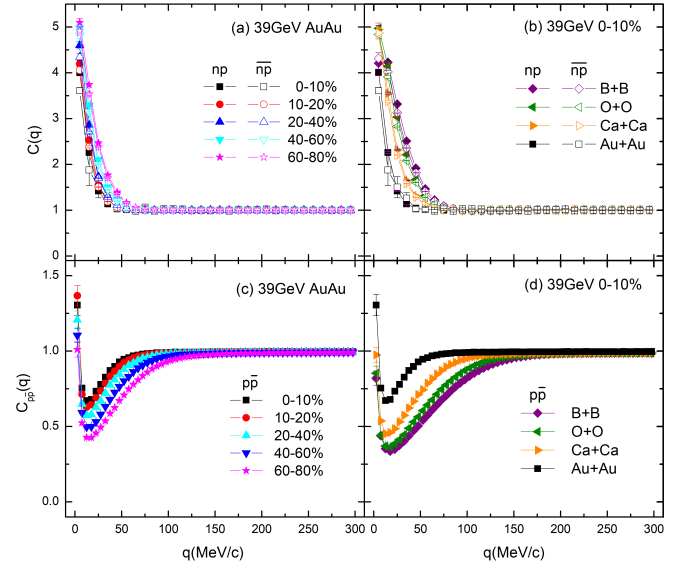

FIG. 4. Similar to Fig. 2 but for the nonidentical particle pairs. (a) (b) n-p momentum correlation functions (solid symbols) and the anti-one (open symbols), (c) (d) p-$\bar{p}$ momentum correlation functions (solid symbols).

The antideuteron−antideuteron momentum correlation function also shows an exact similar shape with deuteron pairs due to the similar phase-space distributions between deuteron and antideuteron. Due to significant less yields of tritons which induce too large error, the antitriton−antitriton momentum correlation function is not shown in the present work, which should be observed as the same trend with triton pairs. Fig. 3 (a) and (c) also compare five centralities of $0-10$ %, $10-20$ %, $20-40$ %,
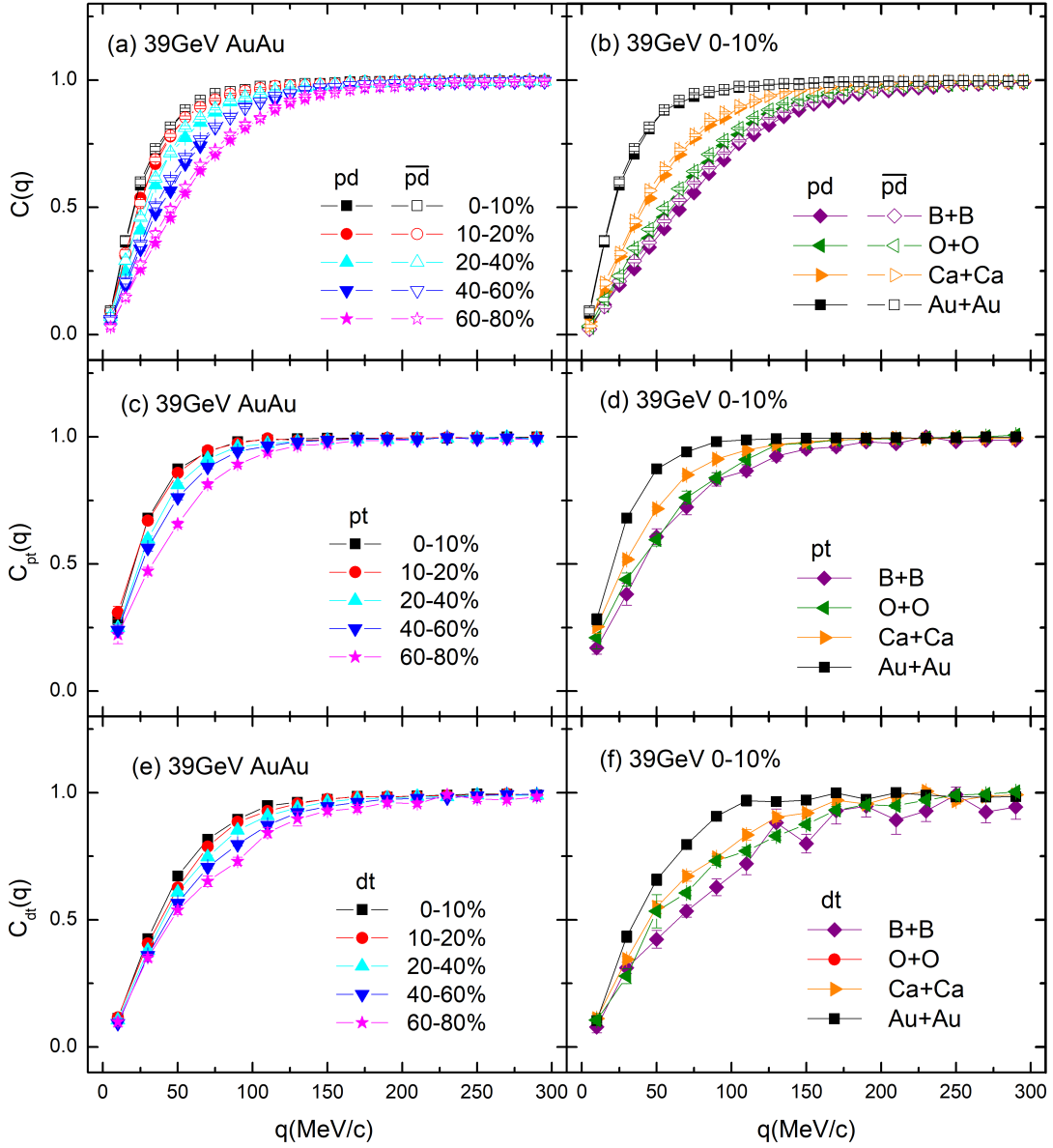
FIG. 5. Similar to Fig. 4 but for nonidentical light (anti)nuclei. (a) (b) p-d momentum correlation functions (solid symbols) and the anti-one (open symbols). (c) (d) p-t momentum correlation functions (solid symbols), (e) (f) d-t momentum correlation functions (solid symbols).

$40 - 60$ %, and $60 - 80$ % for the momentum correlation functions of two light (anti)clusters. The more suppression of the d-d ($\bar{d}$-$\bar{d}$) and t-t correlation functions is clearly visible in peripheral selection. These results also indicate that light (anti)cluster emission occurs from a source of smaller space$-$time extent for peripheral collision, which is the similar to Fig. 2 (a) and (c). In Fig. 3 (b) and (d), an enhancement strength of the momentum correlation function for d-d ($\bar{d}$-$\bar{d}$) and t-t is also observed when light (anti)cluster pairs emitted from smaller systems. However, for small systems such as B and O, the sensitivity seems disappear.

C. Nonidentical light (anti)nuclei momentum correlation functions gated on centrality and system-size

Now we investigate centrality and system-size dependence of the nonidentical (anti)particle momentum correlation functions, such as n-p ($\bar{n}$-$\bar{p}$), p-$\bar{p}$, p-d ($\bar{p}$-$\bar{d}$), p-t and d-t. Fig. 4 (a) and (c) show results for the momentum correlation functions of n-p ($\bar{n}$-$\bar{p}$) and p-$\bar{p}$ for the same centrality classes as Fig. 2. The same centrality dependence is also clearly seen in Fig. 4 (a) and (c). Because of the strong attractive final state interaction between n and p, the n-p ($\bar{n}$-$\bar{p}$) momentum correlation functions
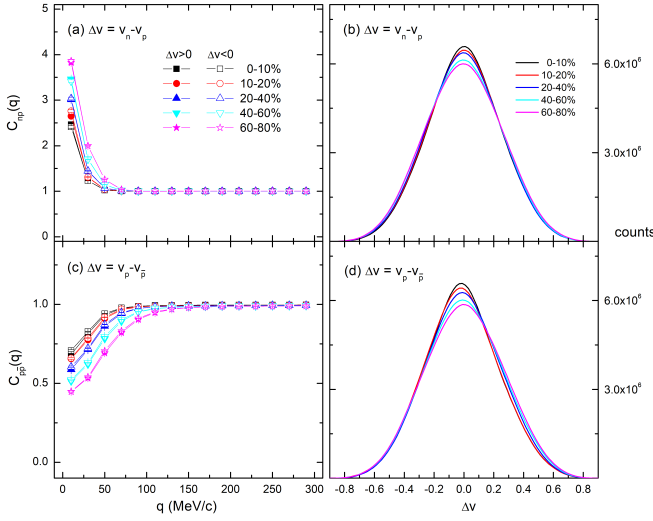
FIG. 6. The velocity-gated momentum correlation functions in relative momentum (left) and velocity difference (Δv) spectra (right) for n-p and p-$\bar{p}$ as a function of five different centralities at mid-rapidity ($|y| < 0.5$) in $\sqrt{s_{NN}} = 39$ GeV $_{79}^{197}$Au$+_{79}^{197}$Au collision. The velocity conditions are indicated in each panel, $\Delta v > 0$ (solid symbols) and the anti-one (open symbols).
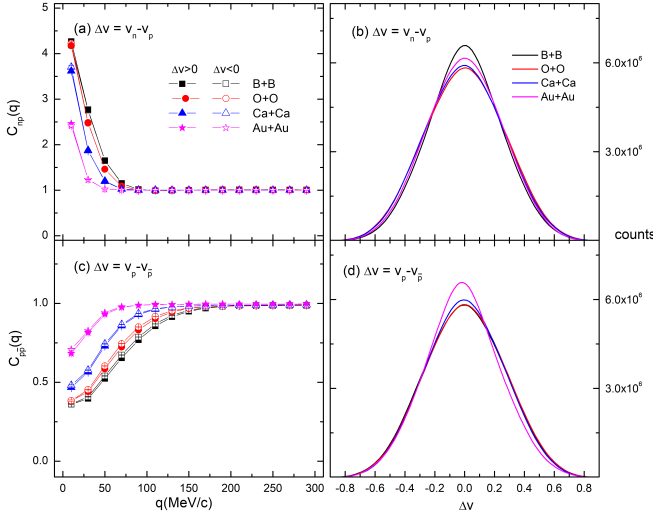

FIG. 7. The velocity-gated momentum correlation functions in relative momentum (left) and velocity difference (Δv) spectra (right) of n-p and p-$\bar{p}$ pairs for $0 - 10$ % central collisions of $_5^{10}$B$+_5^{10}$B, $_8^{16}$O$+_8^{16}$O, $_{20}^{40}$Ca$+_{20}^{40}$Ca as well as $_{79}^{197}$Au$+_{79}^{197}$Au systems at $\sqrt{s_{NN}} = 39$ GeV. The velocity conditions are indicated in each panel, $\Delta v > 0$ (solid symbols) and the anti-one (open symbols).

show a strong positive correlation for small values of the relative momentum q in Fig. 4 (a) and (b). Fig. 4 (c) shows results for proton−antiproton momentum correlation functions, which are different from the results for proton pairs in Fig. 2 (c), however, qualitatively agrees to the experimental results in Ref. [78, 79]. In addition,
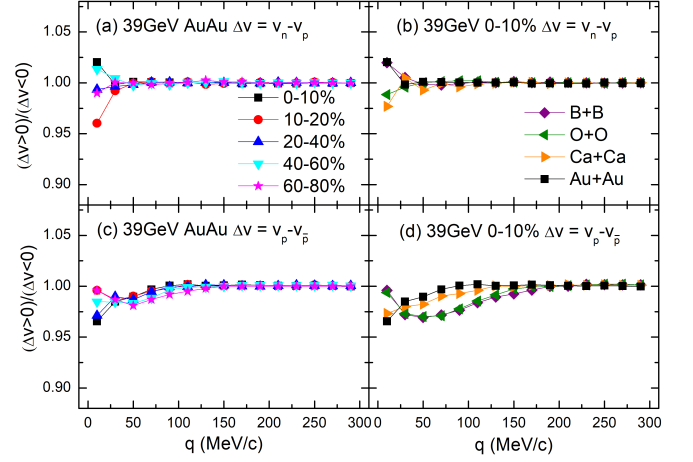

FIG. 8. Ratios of the velocity-gated momentum correlation functions in relative momentum (left) of n-p (a) and p-$\bar{p}$ (c) pairs as a function of five different centralities at mid-rapidity ($|y| < 0.5$) in $\sqrt{s_{NN}} = 39$ GeV $_{79}^{197}$Au$+_{79}^{197}$Au collision. Ratios of the velocity-gated momentum correlation functions in relative momentum (right) of n-p (b) and p-$\bar{p}$ (d) pairs for $0 - 10$ % central collisions of $_5^{10}$B$+_5^{10}$B, $_8^{16}$O$+_8^{16}$O, $_{20}^{40}$Ca$+_{20}^{40}$Ca as well as $_{79}^{197}$Au$+_{79}^{197}$Au systems at $\sqrt{s_{NN}} = 39$ GeV.

Fig. 4 (b) and (d) show system-size dependence of n-p ($\bar{n}$-$\bar{p}$) and p-$\bar{p}$ momentum correlation functions, which is almost unanimously with the identical (anti)particle one in Fig. 2 (b) and (d). We can also observe an enhancement strength of particle pairs momentum correlation function in smaller systems. In the same way, we also investigate the effect of different centralities and system-size on the momentum correlation functions of nonidentical light (anti)nuclei. The p-d ($\bar{p}$-$\bar{d}$), p-t and d-t momentum correlation functions in Fig. 5 (a), (c) and (e) are all characterized by an anti-correlation. For the p-d ($\bar{p}$-$\bar{d}$) momentum correlation functions in Fig. 5 (a), the anti-correlation shape is a little unlike to the proton−deuteron momentum correlation function in the intermediate energy heavy-ion collision [34, 35], indicating that a competition between the s-wave attraction and the Coulomb repulsion. The correlation functions of p-t and d-t in Fig. 4 (c) and (e) also display the trend of below unity due to the dominant Coulomb repulsion, which is similar to the previous results in intermediate energy heavy-ion collisions [34, 35]. In Fig. 5 (b), the system-size dependence of p-d ($\bar{p}$-$\bar{d}$) momentum correlation functions is shown, while we can observe an enhancement of p-d ($\bar{p}$-$\bar{d}$) momentum correlation function in smaller systems. In Fig. 5 (d) and (f), the p-t and d-t momentum correlation functions appear more sensitive to system-size only in the large system such as Au and Ca.
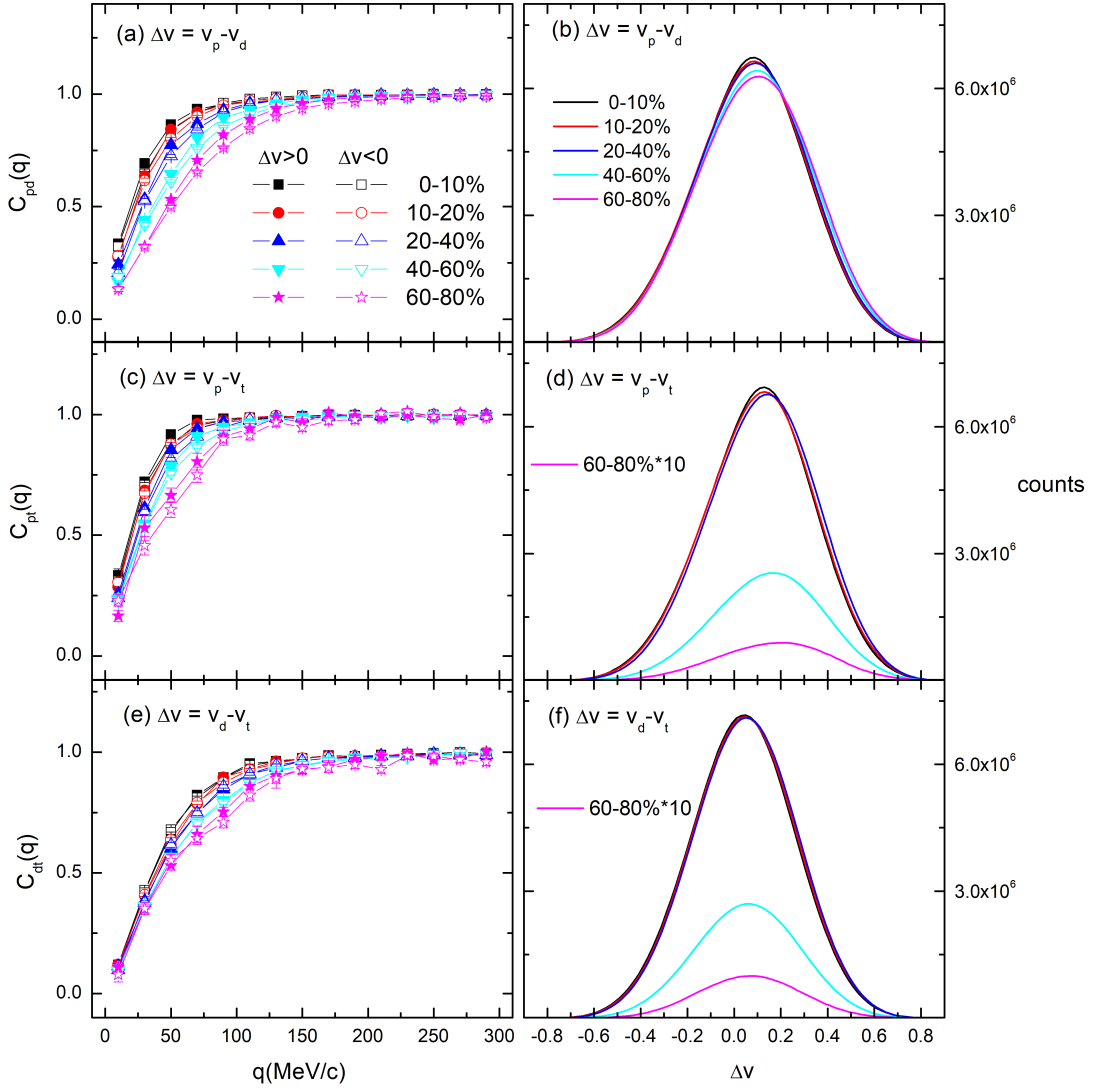
FIG. 9. Similar to Fig. 6 but for p-d (a) (b), p-t (c) (d) and d-t (e) (f) pairs.

D. Velocity selected nonidentical light nuclei momentum correlation functions

The momentum correlation functions of unlike particles can provide an independent constrain on their mean emission order by simply making velocity selections [22, 32, 33, 80, 81]. The principle of comparing the velocity-gated momentum correlation functions for the nonidentical particle pair to infer their average emission order is as follows. Here the two nonidentical particles are named by "a" and "b", respectively. If the velocity of "a" particle is lower than "b" particle, the (anti)correlation will be stronger when the "a" particle is emitted averagely early than the "b" particle, because the space-size between them is reduced during the flight and the final-state interaction (FSI) is enhanced, and vice versa. In addition, the velocity difference (Δv) spectrum between the two nonidentical particles is also sensitive to the mean emission order. Fig. 6 presents the velocity-gated momentum correlation functions and velocity difference (Δv) spectra of unlike particles pairs n-p and p-$\bar{p}$ for $^{197}_{79}\text{Au} + ^{197}_{79}\text{Au}$ collisions at different centralities of $0 - 10$ %, $10 - 20$ %, $20 - 40$ %, $40 - 60$ %, and $60 - 80$ % at $\sqrt{s_{NN}} = 39$ GeV. In Fig. 6 (a) and (c), the centrality dependence on the velocity-gated momentum correlation functions of n-p and p-$\bar{p}$ are similar to Fig. 4. In Fig. 6 (a), the momentum correlation function for n-p pair with $v_n > v_p$ is similar to one with the reverse situation. The symmetry of velocity difference (Δv) spectra for n-p pairs is shown in Fig. 6 (b). The results demonstrates that the average emission sequence of neutrons and protons are almost the same and have no sensitive to the centrality. In Fig. 6 (c), the momentum correlation function for p-$\bar{p}$ pair with $v_p > v_{\bar{p}}$ is slight higher than one with the reverse situation. The slight asymmetry of velocity difference (Δv) spectra for p-$\bar{p}$ pairs is shown in Fig. 6 (d). The corresponding relation indicates that the mean order of emission sequence between pro-
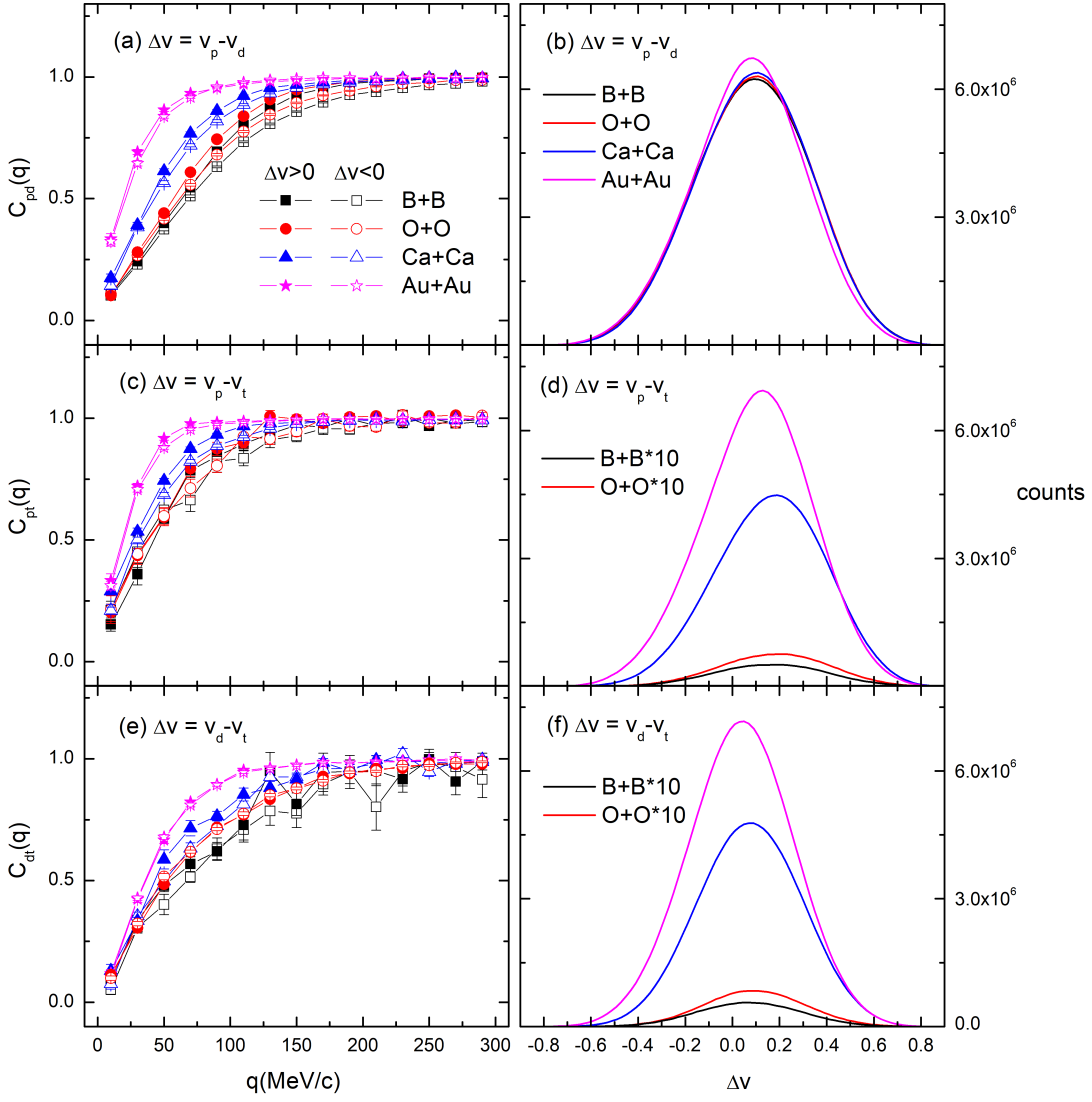
FIG. 10.   Similar to Fig. 7 but for p-d (a) (b), p-t (c) (d) and d-t (e) (f) pairs.

ton and antiproton may be a little different and have also no sensitive to the centrality. In Fig. 7 (a), the momentum correlation functions for n-p pairs with $v_n > v_p$ are always similar to one with the reverse situation with increasing system-size. The symmetry of velocity difference (Δv) spectra for n-p pairs in different systems is shown in Fig. 7 (b). The comparison of velocity-gated momentum correlation functions indicates that the average emission sequence between neutrons and protons can be always identical for different centrality and system-size, which are also shown by their ratios in Fig. 8 (a) and (b). In Fig. 7 (c) and (d), the comparison of velocity-gated momentum correlation functions for p-$\bar{p}$ indicates that the mean order of emission sequence between protons and antiprotons may be a little different and has no dependence on system-size, which are also shown by their ratios in Fig. 8 (c) and (d).

Fig. 9 and Fig. 10 also show centrality and system-size dependence of velocity-gated momentum correlation functions and velocity difference (Δv) spectra of p-d, p-t and d-t pairs, respectively. For p-d and p-t pairs, the momentum correlation functions with $v_p < v_d$ ($v_p < v_t$) is stronger than the one with the reverse situation $v_p > v_d$ ($v_p > v_t$) in Fig. 9. The comparison of the two anti-correlation strengths gives that the mean order of emission that protons are emitted averagely earlier than deuterons and tritons according to the above criteria. The similar trend for d-t pairs is not obviously, where the momentum correlation function with $v_d < v_t$ is stronger and deuterons are emitted averagely earlier than tritons especially in peripheral collision. However, the average emission sequence of protons, deuterons, and tritons is opposite to the emission order in previous results for the intermediate energy heavy-ion collisions [11, 34, 35, 80]. At the same time, Fig. 9 presents velocity difference spectra for p-d, p-t and d-t pairs, respectively. The velocity
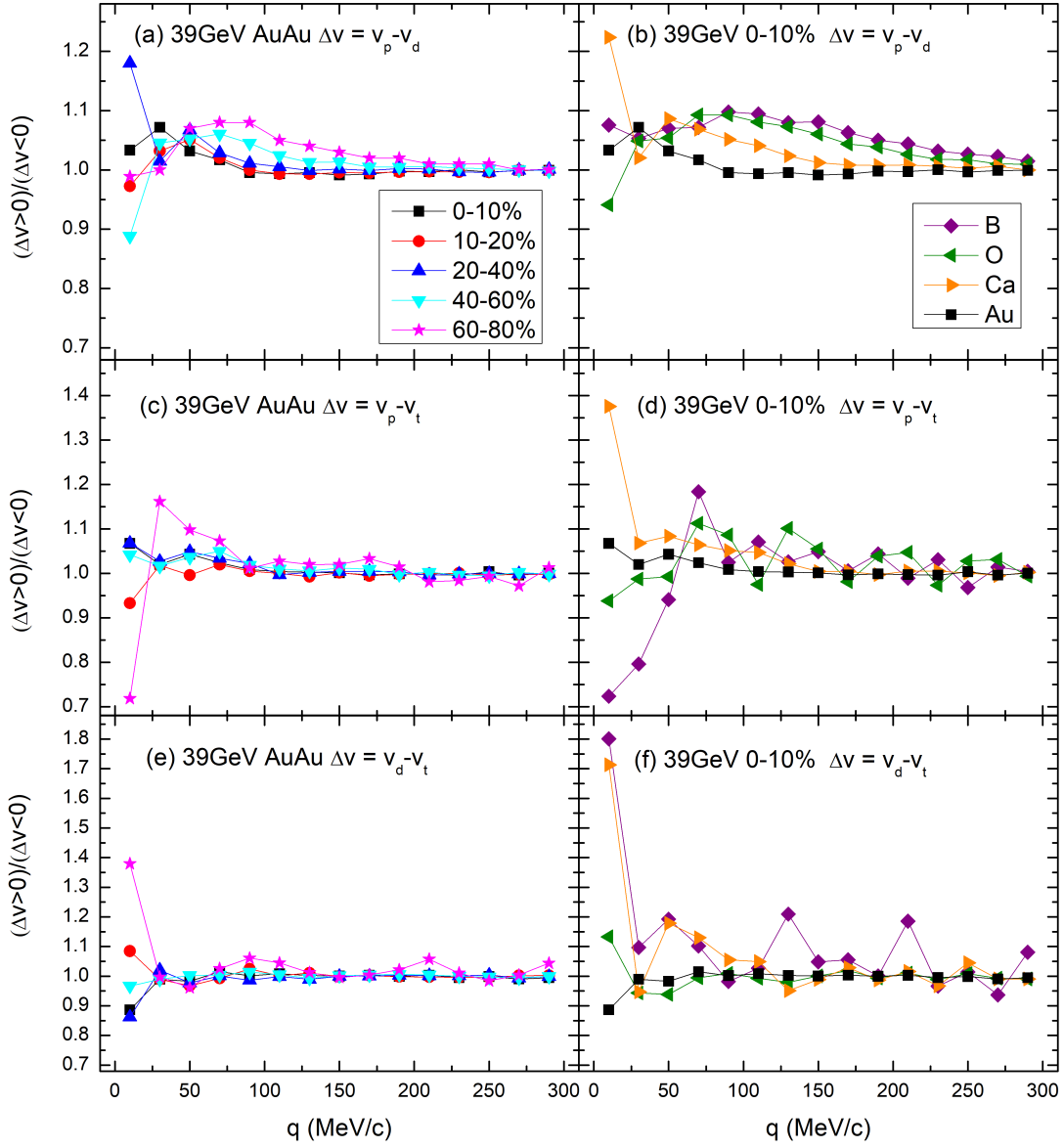
FIG. 11. Similar to Fig. 8 but for *p-d* (a) (b), *p-t* (c) (d) and *d-t* (e) (f) pairs.

difference spectra are all asymmetric due to the mean emission order. In addition, an enhancement difference between the momentum correlation functions for *p-d* (*p-t* or *d-t*) pairs with $v_p > v_d$ ($v_p > v_t$ or $v_d > v_t$) and ones on the reverse situation with larger centrality, which manifests the larger interval of the mean emission order for unlike light nuclei in peripheral collisions. Their ratios in Fig. 11 (a), (c) and (e) can also illustrate the above phenomenon. The system-size dependence for *p-d*, *p-t* and *d-t* pairs can be found that the momentum correlation function with $v_p < v_d$ ($v_p < v_t$ or $v_d < v_t$) is stronger than the one with the reverse situation $v_p > v_d$ ($v_p > v_t$ or $v_d > v_t$) in Fig. 10. Correspondingly, the velocity difference spectra for *p-d*, *p-t* and *d-t* pairs are all asymmetric about $\Delta v = 0$ caused by the average emission order in Fig. 10. Therefore, protons are emitted averagely

earliest and deuterons are emitted averagely earlier than tritons in smaller system-size collision. The system-size dependence of the velocity-gated momentum correlation functions is also clearly seen by their ratios in Fig. 11. With decreasing system-size, we can also observe an enhancement difference between the momentum correlation functions for *p-d* (*p-t* or *d-t*) pair with $v_p > v_d$ ($v_p > v_t$ or $v_d > v_t$) and one with the reverse situation in Fig. 11 (b), (d) and (f).

IV. SUMMARY

In summary, with the AMPT model complemented by the Lednický and Lyuboshitz analytical method, we have constructed the momentum correlation functions of

light (anti)nuclei formed by the coalescence mechanism of (anti)nucleons at different centrality and system-size in $\sqrt{s_{NN}} = 39$ GeV heavy-ion collisions. We present a comparison of proton−proton and proton−antiproton momentum correlation functions with the experimental data from the RHIC-STAR collaboration [78, 79]. Taking the same transverse momentum and rapidity phase space coverage corresponding to the experimental situation as well as the maximum hadronic rescattering time of 700 fm/c in AMPT, it is found that the p-p and p-$\bar{p}$ momentum correlation functions simulated by the present model can match the experimental data. We further study centrality and system-size dependence of momentum correlation functions for identical and non-identical light (anti)nuclei pairs, respectively, which is in the condition of the maximum hadronic rescattering time of 100 fm/c in AMPT. The shape of momentum correlation functions for light (anti)nuclei pairs is consistent with previous works [13, 28, 34, 35, 78, 79], which is caused by both QS and FSI. The similar structure between light nuclei momentum correlation functions and anti-ones indicates that the interaction between them are the same, which has been confirmed in Ref. [28] only about proton and antiproton. The centrality dependence of momentum correlation functions for light (anti)nuclei is investigated by $^{197}_{79}$Au $+^{197}_{79}$ Au collisions at different five centralities of $0 - 10$ %, $10 - 20$ %, $20 - 40$ %, $40 - 60$ %, and $60 - 80$ % at $\sqrt{s_{NN}} = 39$ GeV. It is found that with increasing centralities from center to peripheral, the momentum correlation functions for light (anti)nuclei become stronger, which are probably emitted from smaller source. The momentum correla-

tion functions of light (anti)nuclei are observed sensitive to system-size through studying $^{10}_{5}$B $+^{10}_{5}$ B, $^{16}_{8}$O $+^{16}_{8}$ O, $^{40}_{20}$Ca $+^{40}_{20}$ Ca and $^{197}_{79}$Au $+^{197}_{79}$ Au in central collisions, and the indicated emission source-size of light (anti)nuclei obtained which is self-consistent with their system-size. Momentum correlation functions between nonidentical light nuclei can provide important information about the average emission sequence of them. The average emission time scale between neutrons and protons is almost identical. However, heavier light clusters (deuterons or tritons) are emitted later than protons in the small relative momentum region. In the future we can explore further the energy dependence on the average emission sequence of light nuclei and understand the physical interpretation.

[1] R. Hanbury Brown, R. Q. Twiss, Nature **177**, 27 (1956).
[2] R. Hanbury Brown, R.Q. Twiss, Nature **178**, 1046 (1956).
[3] S. E. Koonin, Phys. Lett. B **70**, 43 (1977).
[4] M. A. Lisa, S. Pratt, R. Soltz, U. Wiedemann, Ann. Rev. Nucl. Part. Sci. **55**, 357 (2005).
[5] U. A. Wiedemann, U. Heinz, Phys. Rep. **319**, 145 (1999).
[6] Gerson Goldhaber, Sulamith Goldhaber, Wonyong Lee, and Abraham Pais, Phys. Rev. **120**, 300 (1960).
[7] A. Bialas et al., Phys. Rev. **62**, 114007 (2000).
[8] R. Ghetti et al., Nucl. Phys. A **674**, 277 (2000).
[9] D. H. Boal, C. K. Gelbke, B. K. Jennings, Rev. Mod. Phys. **62**, 553 (1990).
[10] D. Ardouin, Int. J. Mod. Phys. E **6**, 391 (1997).
[11] R. Ghetti, J. Helgesson, V. Avdeichikov, P. Golubev, B. Jakobsson, N.Colonna, G. Tagliente et al., Phys. Rev. Lett. **91**, 092701 (2003).
[12] J. J. He, S. Zhang, Y. G. Ma, J. H. Chen, C. Zhong, Eur. Phys. J. A **56**, 52 (2020).
[13] Ting-Ting Wang, Yu-Gang Ma, Chun-Jian Zhang, and Zheng-Qiao Zhang, Phys. Rev. C **97**, 034617 (2018).
[14] R. Kotte et al., Eur. Phys. J. A, **23**, 271-278 (2005).
[15] J. Pochodzalla, C. K. Gelbke, W. G. Lynch, M. Maier, D. Ardouin, H. Delagrange et al., Phys. Rev. C **35**, 1695 (1987).
[16] W. G. Gong, W. Bauer, C. K. Gelbke, and S. Pratt, Phys. Rev. C **43**, 781 (1991).
[17] Y. G. Ma, Y. B. Wei, W. Q. Shen, X. Z. Cai, J. G. Chen, J. H.Chen et al., Phys. Rev. C **73**, 014604 (2006).
[18] R. Ghetti, V. Avdeichikov, B. Jakobsson, P. Golubev, J. Helgesson, N. Colonna, G. Tagliente et al., Phys. Rev. C. **69**, 031605(R) (2004).
[19] L. W. Chen, V. Greco, C. M. Ko, and B. A. Li, Phys. Rev. Lett. **90**, 162701 (2003).
[20] D. Q. Fang, Y. G. Ma, X. Y. Sun, P. Zhou, Y. Togano, N. Aoi et al., Phys. Rev. C **94**, 044621 (2016).
[21] B. S. Huang, Y. G. Ma, Phys. Rev. C **101**, 034615 (2020).
[22] D. Gourio et al., Eur. Phys. J. A **7**, 245 (2000).
[23] Lei Shen, Bo-Song Huang, and Yu-Gang Ma, Phys. Rev. C **105**, 014603 (2022).
[24] Ting-Ting Wang, Yu-Gang Ma, De-Qing Fang, and Huan-Ling Liu, Phys. Rev. C **105**, 024620 (2022).
[25] L. M. Fang,Y. G. Ma, S. Zhang, Euro. Phys. J. A **58**, 81 (2022).
[26] J. Adams et al. (STAR Collaboration), Phys. Rev. Lett. **93**, 012301 (2004) .
[27] C. Adler et al. (STAR Collaboration), Phys. Rev. Lett. **87**, 082301 (2001).

[28] L. Adamczyk *et al.* (STAR Collaboration), Nature **527**, 345 (2015).

[29] L. Adamczyk *et al.* (STAR Collaboration), Phys. Rev. Lett. **114**, 022301 (2015).

[30] J. Adam *et al.* (STAR Collaboration), Phys. Lett. B **790**, 490 (2019).

[31] S. Acharya *et al.* (ALICE Collaboration), Nature **588**, 232 (2020).

[32] C. J. Gelderloos and J. M. Alexander, Nucl. Instrum. Methods. A. **349**, 618 (1994).

[33] R. Lednický, V.L. Lyuboshitz, B. Erazmus, and D. Nouais, Phys. Lett. B **373**, 30 (1996).

[34] Ting-Ting Wang, Yu-Gang Ma, Zheng-Qiao Zhang, Phys. Rev. C **99**, 054626 (2019).

[35] Yijie Wang, Fenhai Guan, Qianghua Wu *et al.*, Phys. Lett. B **825**, 136856 (2022).

[36] Bao-Shan Xi, Zheng-Qiao Zhang, Song Zhang and Yu-Gang Ma, Phys. Rev. C **102**, 064901 (2020).

[37] S. Voloshin, R. *Lednický*, S. Panitkin, and Nu Xu, Phys. Rev. L **79**, 4766 (1997).

[38] D. Ardouin *et al.*, Phys. Lett. B **446**, 191 (1999).

[39] R. Kotte *et al.*, Eur. Phys. J. A, **6**, 185 (1999).

[40] Z.-W. Lin, C. M. Ko, B.-A. Li, B. Zhang, and S. Pal, Phys. Rev. C **72**, 064901 (2005).

[41] Z. W. Lin and L. Zheng, Nucl. Sci. Tech. **32**, 113 (2021).

[42] L. W. Chen, C. M. Ko, and B. A. Li, Nucl. Phys. A **729**, 809 (2003).

[43] S. Zhang, J. H. Chen, H. Crawford, D. Keane, Y. G. Ma, and Z. Xu, Phys. Lett. B **684**, 224 (2010).

[44] Yi-Lin Cheng, Song Zhang and Yu-Gang Ma, Eur. Phys. J. A, **57**, 330 (2021).

[45] R. Lednický, Nucl. Phys. A **774**, 189 (2006).

[46] R. Lednický, Phys. Part. Nucl. **40**, 307 (2009).

[47] R. Lednický, Phys. Ato. Nucl. **71**, 1572 (2008).

[48] R. Lednický, Braz. J. Phys. **37**, 939 (2007).

[49] B. Alver, G. Roland, Phys. Rev. C **81**, 054905 (2010).

[50] G. L. Ma, X. N. Wang, Phys. Rev. Lett. **106**, 162301 (2011).

[51] L. X. Han, G. L. Ma, Y. G. Ma, X. Z. Cai, J. H. Chen, S. Zhang, C. Zhong, Phys. Rev. C **84**, 064907 (2011).

[52] A. Bzdak, G. L. Ma, Phys. Rev. Lett. **113**, 252301 (2014).

[53] S. Zhang, Y. G. Ma, J. H. Chen, W. B. He, C. Zhong, Phys. Rev. C **95**, 064904 (2017).

[54] Zheng-Qiao Zhang, Song Zhang and Yu-Gang Ma, Chinese Phys. C **38**, 014102 (2014).

[55] H. Zhang, J. F. Liao, E. K. Wang, Q. Wang, H. X. Xing, Phys. Rev. Lett. **126**, 012301 (2021).

[56] H. Wang, J. H. Chen, Nucl. Sci. Tech. **32**, 2 (2021).

[57] H. Wang, J. H. Chen, Nucl. Sci. Tech. **33**, 15 (2022).

[58] X.-N. Wang and M. Gyulassy, Phys. Rev. D **44**, 3501 (1991).

[59] M. Gyulassy and X.-N. Wang, Computer Physics Communications **83**, 307 (1994).

[60] B. Zhang, Computer Physics Communications **109**, 193 (1998).

[61] Zi-wei Lin, Subrata Pal, C. M. Ko, Bao-An Li, and Bin Zhang, Phys. Rev. C **64**, 011902(R) (2001).

[62] Subrata Pal, C. M. Ko, Zi-Wei Lin, Nucl. Phys. A **730**, 143 (2004).

[63] Subrata Pal, C. M. Ko, Zi-Wei Lin, Nucl. Phys. A **707**, 525 (2002).

[64] B. A. Li and C. M. Ko, Phys. Rev. C **52**, 2037 (1995).

[65] L. Csernai and J. I. Kapusta, Physics Reports **131**, 223 (1986).

[66] Jinhui Chen, Declan Keane, Yu-Gang Ma, Aihong Tang, Zhangbu Xu, Physics Reports **760**, 1 (2018).

[67] Lie-Wen Chen, C. M. Ko, and Bao-An Li, Phys. Rev. C **68**, 017601 (2003).

[68] M. Gyulassy *et al.*, Nucl. Phys. A **402**, 596 (1983).

[69] J. Aichelin, A. Rosenhauer, G.Peilert, H. Stoecker, W.Greiner, Phys. Rev. Lett. **58**, 1926 (1987).

[70] Volker Koch *et al.*, Phys. Lett. B **241**, 174 (1990).

[71] P. Pawlowski *et al.*, Eur. Phys. J. A **9**, 371 (2000).

[72] R. Mattiello, H. Sorge, H. Stocker, W. Greiner, Phys. Rev. C **55**, 1443 (1997).

[73] J.L. Nagle, B. S. Kumar, D. Kusnezov, H. Sorge, R. Mattiello, Phys. Rev. C **53**, 367 (1996).

[74] K. J. Sun and L.-W. Chen, Phys. Lett. B **751**, 272 (2015).

[75] R. Lednický, V.L. Lyuboshitz, Sov. J. Nucl. Phys. **35**, 770 (1982).

[76] B. Erazmus, L. Martin, R. Lednicky, N. Carjan, Phys. Rev. C **49**, 349 (1994).

[77] J. Arvieux, Nucl. Phys. A **221**, 253 (1974).

[78] H.P. Zbroszczyk, Acta Phys. Pol. B Proc. Suppl. **12**, 205 (2019).

[79] Sebastian Siejka (STAR Collaboration), Nucl. Phys. A **982**, 359 (2019).

[80] C. J. Gelderloos, R. Sun, N. N. Ajitanand, J. M. Alexander, E. Bauge, A. Elmaani *et al.*, Phys. Rev. C **52**, R2834 (1995).

[81] Bo-Song Huang, Yu-Gang Ma, Chin. Phys. C **44**, 094105 (2020).